Investigating the Impact of Varied C-Rates on Lithium-Ion Batteries: A 1D Simulation Study

Journal of Physics: Conference Series **2893** (2024) 012050 doi:10.1088/1742-6596/2893/1/012050

Investigating the Impact of Varied C-Rates on Lithium-Ion Batteries: A 1D Simulation Study

Elif Kaya[1*], Luca Reina[1], Alessandro d'Adamo[1]

[1] Dipartimento di Ingegneria Enzo Ferrari, Università degli Studi di Modena e Reggio Emilia, Modena 41125, Italy

*Correspondence address. E-mail: elif.kaya@unimore.it

Abstract. With the advancement of powertrain technology and progressive vehicle electrification, one of the solutions for the growing need for energy storage is batteries. A secondary battery is a device that stores electrical energy in chemical form and delivers it as electrical energy when needed (discharging), with the possibility to revert the process converting electrical to chemical energy (charging). The lithium-ion battery type used in the study offers increased energy and power density with a cell voltage of approximately 3.6 V, making it suitable for use in portable electronic devices like mobile phones and laptops. In this research, a 1D model (through-electrolyte direction) of lithium-ion battery was analysed, in which the effect of different C-rates was investigated using the battery and design module of COMSOL Multiphysics software for 0.1C, 0.5C, 1C, 2C, and 3C rates, relevant for automotive applications. The simulation results of the lithium-ion battery model constitute an important step towards the development of battery technology, allowing an understanding of the transport processes in the electrodes and electrolyte. The results revealed that under higher C-rates of operation, differences emerge in electrolyte and electrode voltage ranges, salt concentration profiles in the electrolyte, surface and center electrode particle lithium concentrations.

1. Introduction

Energy production and storage systems are one of the most fundamental and important needs of the planet Earth. Since the industrial revolution, there has been a notable rise in global energy consumption [1]. Understanding and improving batteries, which are one of the main components of energy systems, is a crucial step to take for the future. A battery is composed of multiple interconnected electrical cells, each of which transforms chemical energy into electrical energy. These cells are composed of positive and negative electrodes isolated by an electrolytic separator, and the electrochemical reactions developing at the electrodes generates a direct-current (DC) electricity. Battery types span from lead acid, nickel iron, nickel cadmium, nickel metal hydride, lithium-ion, lithium polymer, lithium iron, sodium sulfide, and sodium metal chloride, depending on the electrode or electrolyte used in the batteries [2]. The lithium-ion battery used in this study is a rechargeable type of battery that utilizes the reversible reduction of lithium ions for energy storage. In conventional lithium-ion batteries, the anode (negative electrode) is typically made of graphite, while the cathode (positive electrode) is usually a lithium metal oxide. The electrolyte commonly consists of lithium salt dissolved in an organic solvent [3, 4]. Lithium-ion batteries are used in various applications, including the military, aviation, and numerous electronic devices such as computers and phones [5].

When reviewing the literature, it is evident that many articles discuss the impact of C-rate on lithium-ion batteries. The C-rate is a relative measure of cell current, and the metric is based on the constant

current during charge or discharge that the cell can sustain for one hour (defined as 1C), hence expressing the relationship between the battery's capacity and the current. Leißing et al. [6] discovered that the gassing dependence on the C-rate relies on the type of graphite material used. According to the Snyder study [7], at elevated C-rates deterioration occurs due to both chemical and mechanical factors, with mechanical degradation becoming more prominent as the C-rate rises. Higher charging rates have an adverse impact on battery lifespan: charging beyond 4C leads to alterations in the chemical composition, causing substantial damage and reducing the battery's longevity, as found by Somerville et al. [8]. As per Wang et al. study [9], experimental findings showed that the capacity degradation was significantly influenced by time and temperature, although it was minimally affected by charging rates. Tran et al. [10] examined the electrochemical behaviour of lithium-ion graphite electrodes with particle diameters ranging from 6 to 44 μm at various discharge (intercalation)/charge (deintercalation) rates, from C to C/60. Both the average particle size and rate affect the electrode capacity related to the physical and chemical characteristics of the graphite particles. The paper by Li et al. [11] demonstrates that the average absolute discrepancies in terminal voltage for lithium cobalt oxide ($LiCoO_2$) batteries remained below 30 mV at discharge rates below 2C and below 50 mV up to a 4C discharge rate, which was the maximum limit in their testing. For lithium iron phosphate ($LiFePO_4$) batteries, the average absolute discrepancies stayed under 22 mV at discharge rates up to 4C and remained within 50 mV at 5C. Zheng et al. [12] suggest that a power-law correlation is established between the maximum operational C-rate and the loading of electrodes. The rise in specific resistance as electrode thickness increases is not a significant contributor to the inferior rate performance of thicker electrodes. This power-law connection is characteristic of a system dependent on diffusion, suggesting that the rate-limiting step for the discharge process is the diffusion of Li ions within the electrode. In this study, the effects of five different C rates (0.1C, 0.5C, 1C, 2C, 3C) were investigated on the simulation results of 1D lithium-ion battery models modelled in the COMSOL Multiphysics CFD software.

2. Materials and Methods

2.1 Physical and Chemical Properties

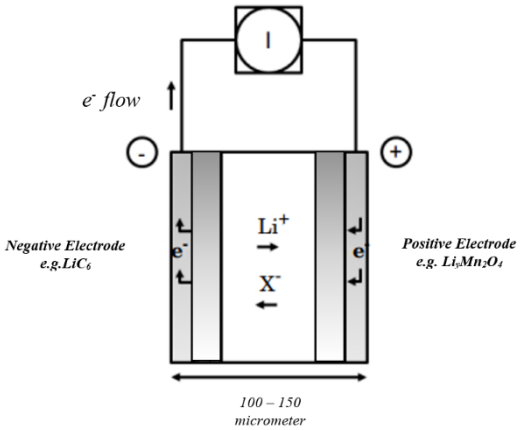

Figure 1. The internal structure of a lithium-ion battery, from [13]

Figure 1 shows the schematic illustration of the lithium-ion battery. The graphite intercalation compound (LiC_6) is used as the negative electrode, while the positive electrode is composed of lithium manganese oxide (LMO). It should be noted that alternative materials may also be utilized for both electrodes. During discharge, lithium ions move from the anode through the electrolyte to the cathode. On the contrary, while charging, an external power supply compels electrons to travel from the cathode to the anode.

The chemical reactions occurring at the negative electrode during both charging and discharging phases are described in the following equations [14]. In the given equations, the variable "x" represents the number of lithium ions (Li^+) and electrons (e^-) involved in the reaction per formula unit of the graphite structure (C_6).

$$Li_xC_6 \rightarrow 6C + xLi^+ + xe^- \quad (1)$$

$$6C + xLi^+ + xe^- \rightarrow Li_xC_6 \quad (2)$$

The chemical reactions taking place at the positive electrode throughout the charging and discharging phases are outlined in [14]:

$$Li_{1-x}Mn_2O_4 + xLi^+ + xe^- \rightarrow LiMn_2O_4 \quad (3)$$

$$LiMn_2O_4 \rightarrow Li_{1-x}Mn_2O_4 + xLi^+ + xe^- \quad (4)$$

The model is one-dimensional in geometry (through-electrolyte direction), and it maintains isothermal conditions. The material characteristics correspond to those commonly found in lithium-ion batteries. The electrolyte comprises a solution of 2 M lithium hexafluorophosphate ($LiPF_6$) salt in a 1:2 volume ratio of ethylene carbonate (EC): dimethyl carbonate (DMC) solvent and Poly (vinylidene Fluoride-Hexafluoropropylene) (p(VDF-HFP)). Carbon-based material is used for the negative electrode, while $LiMn_2O_4$ is employed for the positive electrode [13]. Figure 2 shows the one-dimensional battery geometry with labels identifying its main components. Three main domains were created, namely negative electrode, electrolyte, and positive electrode [15]. The negative electrode, measuring 1×10^{-4} meters in length, followed by an electrolyte spanning 0.52×10^{-4} meters, and finally, a positive electrode with a length of 1.74×10^{-4} meters. This instance depicts the cross-sectional view of the battery in a one-dimensional model, which means that edge effects along the length and height of the battery are neglected in this study.

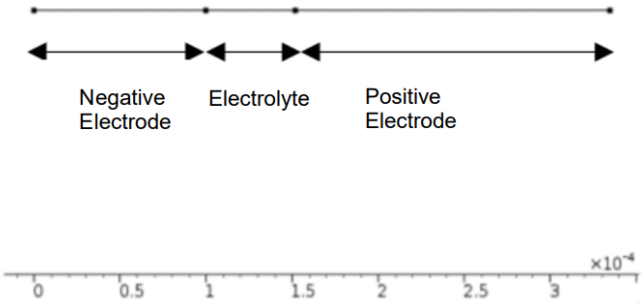

Figure 2. The one-dimensional Li-ion battery model, modified from [15]

The cycle used in this study prescribes discharging for 2000 seconds at the standard current density, followed by 300 seconds of open circuit, then charging for 2000 seconds at the standard current density, and concluding with open circuit conditions [13] relative to a 1C discharge/charge current. Figure 3 shows the change in total discharge/charge current versus time.

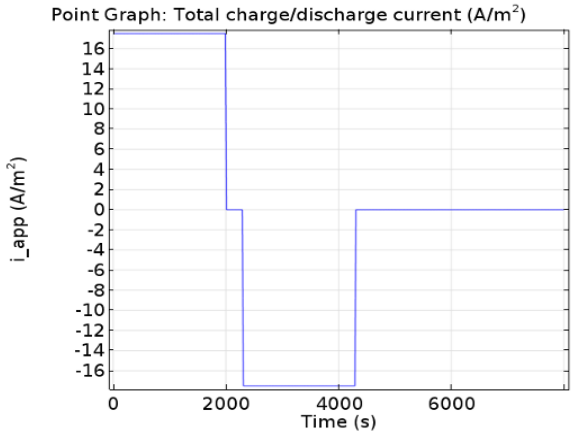

Figure 3. Current cycle used for model testing relative to 1C, from [15]

2.2 Numerical Method

The model encompasses these assumptions:

• Electron flow through the electrodes.

• Movement of ionic charges within the electrodes and electrolyte/separator.

• Diffusive material transfer within the electrolyte, enabling the incorporation of concentration effects on ionic conductivity and concentration over potential, derived from experimental findings.

• Material migration within the spherical particles constituting the electrodes.

• Utilization of Butler-Volmer electrode kinetics based on experimentally determined discharge patterns for the equilibrium potential [13].

The COMSOL Multiphysics model employs multi-dimensional governing equations to simulate transport phenomena, here reduced to a one-dimensional transport type (referred to as x-coordinate). Within the electrolyte region, these governing equations are utilized.

$$\frac{\partial c_l}{\partial t} + \frac{\partial N_l}{\partial x} = R_l \tag{5}$$

$$i_l = -\sigma_l \frac{\partial \emptyset_l}{\partial x} + \frac{2\sigma_l RT}{F}\left(1 + \frac{\partial lnf}{\partial lnc_l}\right)(1 - t_+)\frac{\partial lnc_l}{\partial x} \tag{6}$$

$$N_l = -D_l \frac{\partial c_l}{\partial x} + \frac{i_l t_+}{F} \tag{7}$$

The parameters within these governing equations are elucidated as follows: c_l depicts the electrolyte salt concentration, N_l shows the number of ions, R_l defines the contact resistance between the electrode and current collectors [14]. i_l illustrates the ion transfer current across the electrode, σ_l describes the electric conductivity of the electrolyte, φ_l depicts the electrolyte potential, R shows the universal gas constant, T defines the temperature of the isothermal battery, F illustrates the Faradic constant, ($\partial \ln f$ / $\partial \ln c_l$) describes the activity dependence. ”f”, in this case, is the mean molar activity coefficient, which is assumed to be constant [14]. t_+ depicts the transport number, which is the portion of the total electric current in an electrolyte that is carried by a specific ionic species. D_l shows the diffusion coefficient.

Equation 5 indicates that the alteration in electrolyte salt concentration over time, coupled with the change in the number of ions concerning battery length, equals a constant, representing the contact resistance between the electrode and current collectors. Equation 6 elucidates the flow of electrical current within the battery, illustrating its derivation from both the potential gradient and diffusion due to concentration gradients. As Linden points out [16], the transport number in this context determines the fraction of the electric energy resulting from the displacement of the potential from the equilibrium value, thereby governing the rate of electrochemical transformation. Put simply, it delineates the proportion of lithium ions traversing the separator. Equation 7 defines lithium-ion current flow as the sum of concentration current density and a portion of the net current flow, adjusted accordingly for units.

Within the porous electrode regions, the governing equations are as follows:

$$\frac{\partial \epsilon_l c_l}{\partial t} + \frac{\partial N_l}{\partial x} = R_l \tag{8}$$

$$i_l = -\sigma_{l,eff} \frac{\partial \emptyset_l}{\partial x} + \frac{2\sigma_{l,eff} RT}{F}(1 + \frac{\partial lnf}{\partial lnc_l})(1 - t_+) \frac{\partial lnc_l}{\partial x} \tag{9}$$

$$N_l = -D_{l,eff} \frac{\partial c_l}{\partial x} + \frac{i_l t_+}{F} \tag{10}$$

Here, ε_l represents the volumetric fraction (similar to porosity), $\sigma_{l,\,eff} = \varepsilon_l^{1.5}\sigma_l$ denotes the effective electrical conductivity within the porous electrode, and $D_{l,\,eff} = \varepsilon_l^{1.5} D_l$ signifies the effective diffusivity coefficient within the porous electrode. These effective parameters are employed to consider both porosity and tortuosity. The Bruggeman coefficient, set at 1.5 to simulate a packed bed of spherical particles [13], is a factor used to model alterations in electrical conductivity and diffusivity resulting from closely packed spheres in contact with each other.

2.3 Validation of the Experimental Results

The nominal discharge current density, corresponding to case 1C (a current density corresponding to a theoretical full discharge in one hour), is 17.5 A/m^2. Following the C-rate definition, a 17.5 Ah cell should theoretically be able to deliver 17.5 A (1C) for 1 hour or 1.75 A (C/10) for about 10 hours, although it is known that the relationship is not linear. If the cell is discharged at a 10C rate, it will be completely discharged in about six minutes. The model is based on a study by Doyle et al. [17]. The experimental results were validated for three different C-rates with the numerical model created by COMSOL Multiphysics software battery and design module. As seen in Figure 4, the numerical and experimental results were found to overlap.

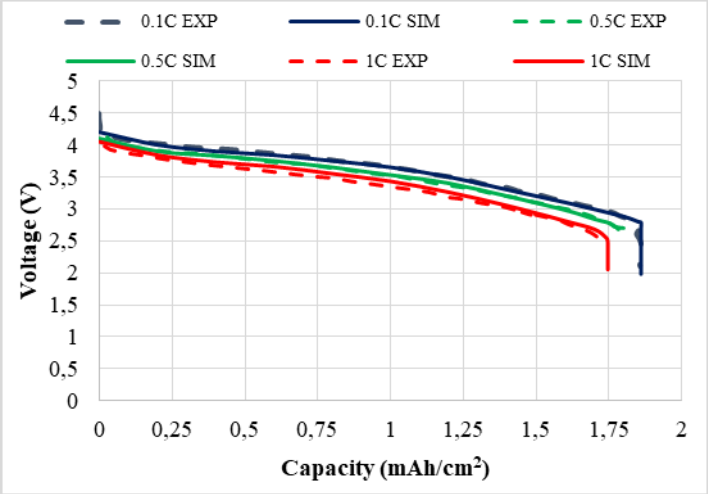

Figure 4. Cell potential (V) vs. capacity (mAh/cm^2) at various discharge rates

3. Results

A 1D isothermal lithium-ion battery is investigated under different C-rates on COMSOL Multiphysics software. Upon examining Figure 5, it is evident that the initial voltage values for all C-rates are approximately 4V and closely aligned. Figure 5 is examined; the initial voltage value is observed to decrease slightly with the increase in the C-rate at the same time. The mentioned voltage values in Figure 5 correspond to those in Figure 4 for the rates of 0.1C, 0.5C, and 1C. The figure also clearly demonstrates that with an increase in the C-rate, the applied battery cell current density proportionally increases, leading to a reduction in discharge-charge durations. In Figure 3, for 1C, the discharge, open circuit, and charge periods are shown as 0-2000, 2000-2300, and 2300-4300 seconds, respectively. Proportional to the C-rate, the changes occurring in these periods are clearly seen in Figure 5. For the 0.1C rate, which represents one-tenth of the 1C rate, the discharge, open circuit, and charge periods will occur ten times slower, respectively: 0-20000, 20000-23000, and 23000-43000 seconds. For the 0.5C rate, which represents half of the 1C rate, the discharge, open circuit, and charge periods will occur twice as slowly, respectively: 0-4000, 4000-4600, and 4600-8600 seconds. For the 2C rate, which represents twice the 1C rate, the discharge, open circuit, and charge periods will occur twice as quickly, respectively: 0-1000, 1000-1150, and 1150-2150 seconds. Finally, for the 3C rate, which represents three times the 1C rate, the discharge, open circuit, and charge periods will occur three times faster, respectively: 0-666.66, 666.66-766.66, and 766.66-1433.33 seconds.

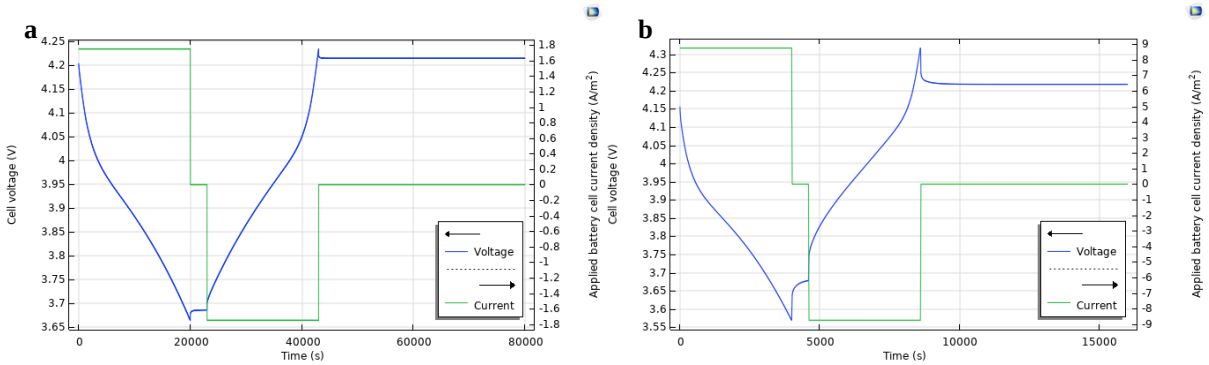

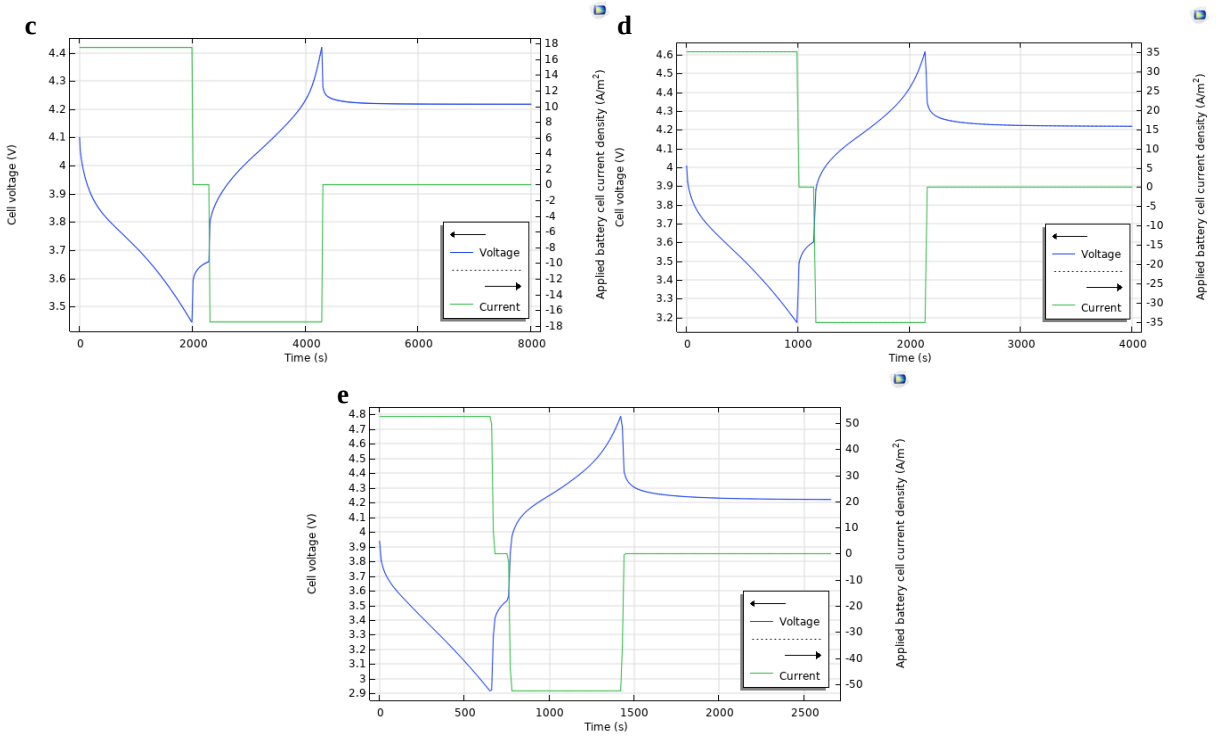

Figure 5. Load cycle voltage and current for five different C-rates: a) 0.1C, b) 0.5C, c) 1C, d) 2C, e) 3C

The time points of 10 s, 100 s, and 300 s, which include in the discharge period for all C-rates as seen in Figure 5, have been selected to accurately compare the data within Figures 6, 7, and 9. When looking at Figure 6 and Table 1, it is observed that the electrolyte voltage decreases over time for all battery components, including the negative electrode, electrolyte, and positive electrode, within the first 300 seconds of the discharge period for all C-rates. According to Figure 6 and Table 1, the rate of decrease in electrolyte voltage over time has increased for all three battery components as the C-rate increases.

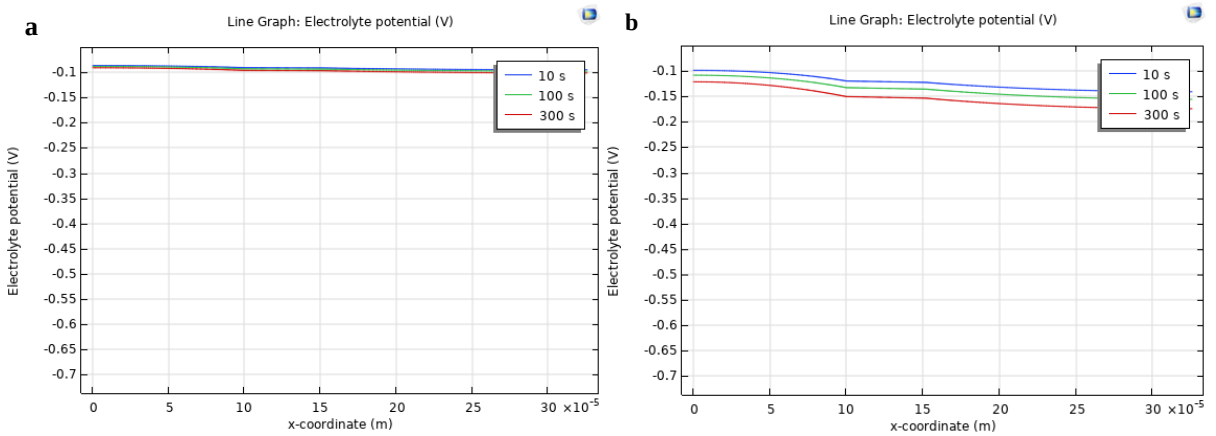

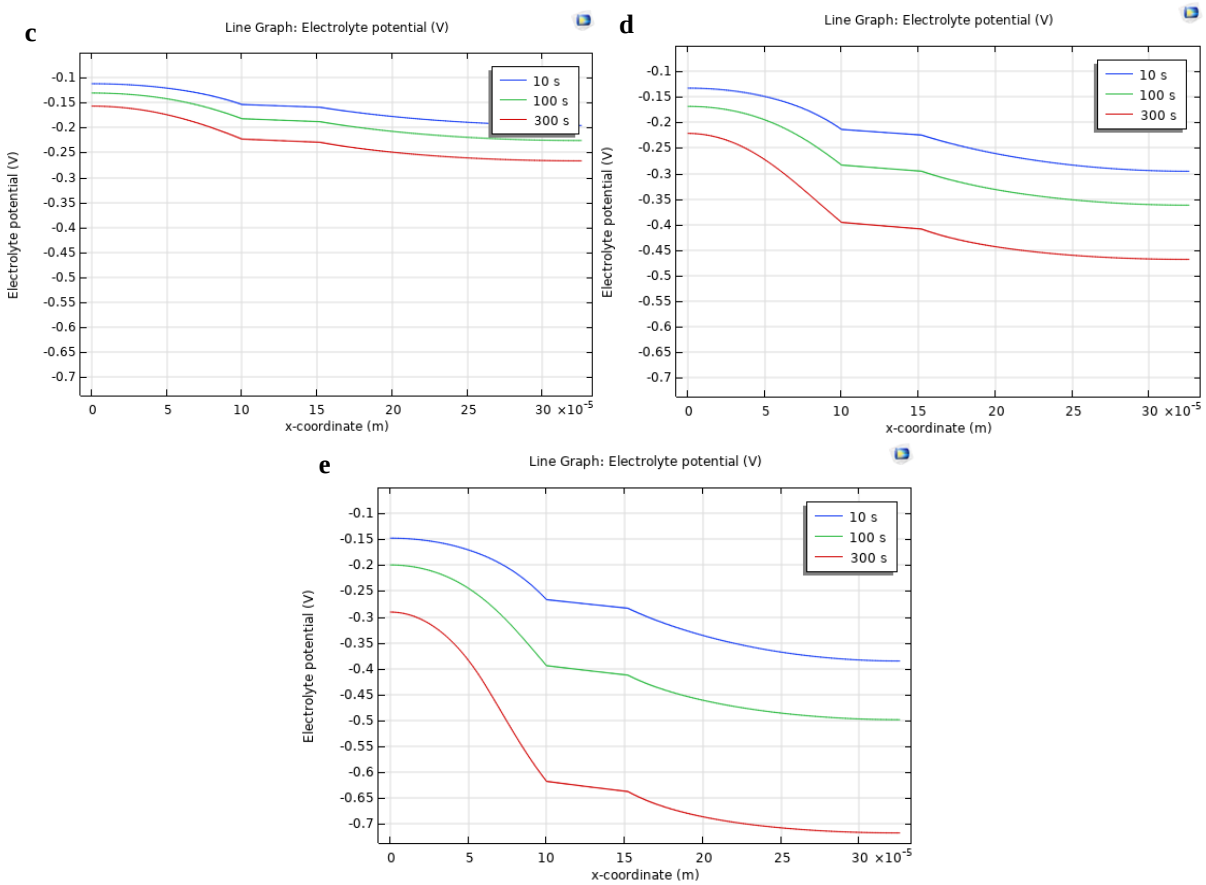

Figure 6. Electrolyte potential for five different C-rates: a) 0.1C, b) 0.5C, c) 1C, d) 2C, e) 3C

Table 1. Between 10s and 300s, the approximate average electrolyte potential difference of battery components for five different C-rates

C-Rate	Between 10s and 300s, Approximate Average Electrolyte Potential Difference of Negative Electrode [0-10]x10^{-5} m	Between 10s and 300s, Approximate Average Electrolyte Potential Difference of Electrolyte [10-15,2]x10^{-5} m	Between 10s and 300s, Approximate Average Electrolyte Potential Difference of Positive Electrode [15,2-32,6]x10^{-5} m
0.1	-0.087 V _ -0.092 V Difference = 0.005 V	-0.091 V _ -0.096 V Difference = 0.005 V	-0.094 V _ -0.1 V Difference = 0.006 V
0.5	-0.103 V _ -0.128 V Difference = 0.025 V	-0.121 V _ -0.152 V Difference = 0.031 V	-0.136 V _ -0.168 V Difference = 0.032 V
1	-0.12 V _ -0.175 V Difference = 0.055 V	-0.157 V _ -0.227 V Difference = 0.07 V	-0.186 V _ -0.257 V Difference = 0.071 V
2	-0.15 V _ -0.273 V Difference = 0.123 V	-0.22 V _ -0.404 V Difference = 0.184 V	-0.276 V _ -0.455 V Difference = 0.179 V
3	-0.17 V _ -0.385 V Difference = 0.215 V	-0.277 V _ -0.63 V Difference = 0.353 V	-0.358 V _ -0.7 V Difference = 0.342 V

According to Figure 7 and Table 2, within the first 300 seconds of the discharge period for all C-rates, the electric potential value of the positive electrode decreases over time. The decline trend in the positive electrode's electric potential over time has increased with the rise in the C rate.

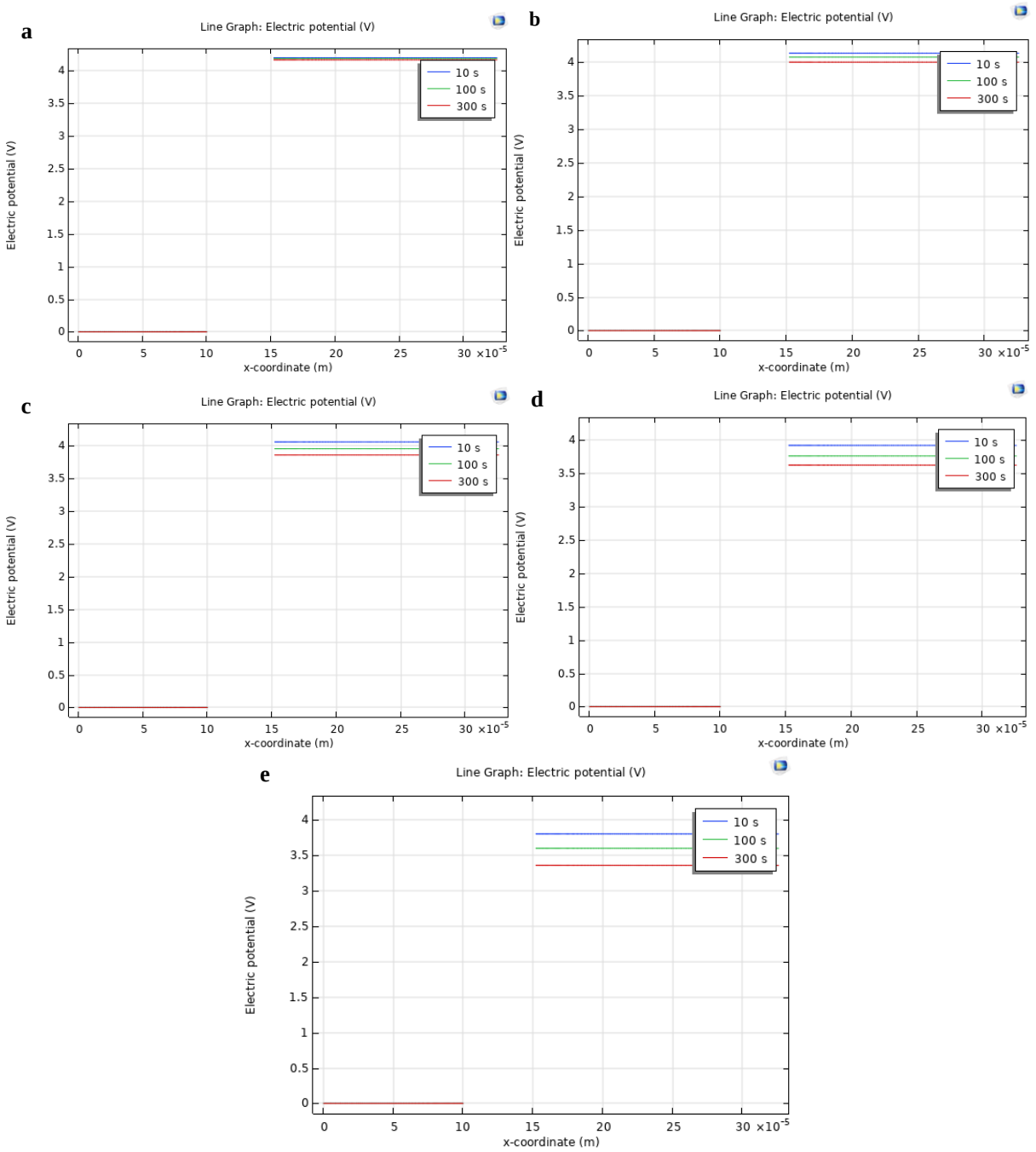

Figure 7. Electrode potential with respect to ground for five different C-rates: a) 0.1C, b) 0.5C, c) 1C, d) 2C, e) 3C

Table 2. Between 10s and 300s, the approximate electric potential difference of the positive electrode for five different C-rates.

C-Rate	Between 10s and 300s, Approximate Electric Potential Difference of Positive Electrode [15,2-32,6]x10^{-5} m
0.1	4.2 V – 4.17 V Difference = 0.03 V
0.5	4.13 V – 4.0 V Difference = 0.13 V
1	4.05 V – 3.85 V Difference = 0.2 V
2	3.92 V – 3.63 V Difference = 0.29 V
3	3.8 V – 3.36 V Difference = 0.44 V

The reason for choosing specific times such as 1200, 1800, 2200, 2400, and 3000 seconds for the graph "Electrolyte salt concentration" is to capture key moments within the battery's charge-discharge cycle for 1C rate. 1200 seconds: This time is within the first half of the discharge phase (2000 seconds). It provides insight into the concentration profile when the battery is actively discharging but not yet close to completion. 1800 seconds: This time is towards the end of the discharge phase. It shows how the concentration profile evolves as the battery nears the end of its discharge cycle, likely highlighting depletion effects. 2200 seconds: This time falls within the rest phase after discharge (300 seconds). It helps in understanding the relaxation behavior of the electrolyte concentration shortly after the discharge ends. 2400 seconds: This time is immediately after the rest phase and at the beginning of the charge phase. It shows how the concentration profile looks as the battery starts charging, providing a baseline for the charging process. 3000 seconds: This time is towards the end of the charge phase (2000 seconds). It captures the electrolyte concentration profile near the end of charging, highlighting how it fills up and redistributes the lithium ions. The selected times of 1200 s, 1800 s, 2200 s, 2400 s, and 3000 s in Figure 8 and Table 3 represent the discharge period for 0.1C and 0.5C rates, while for the 1C rate, 3000 s, and for the 2C rate, 1800 s, 2200 s, 2400 s, and 3000 s represent the charge period. The vertical axis values corresponding to the approximate average coordinates on the horizontal axis for two different time scales at the top and bottom of the selected time lines in all battery components were manually determined to calculate the average electrolyte salt concentration value. As shown in Figure 8, and Table 3, it is evident that the average electrolyte salt concentration range according to time increases with the rise in C-rate for all three battery components. When the circuit demands a significant amount of current, a considerably greater difference in potential between the positive and negative electrodes will be observed [15].

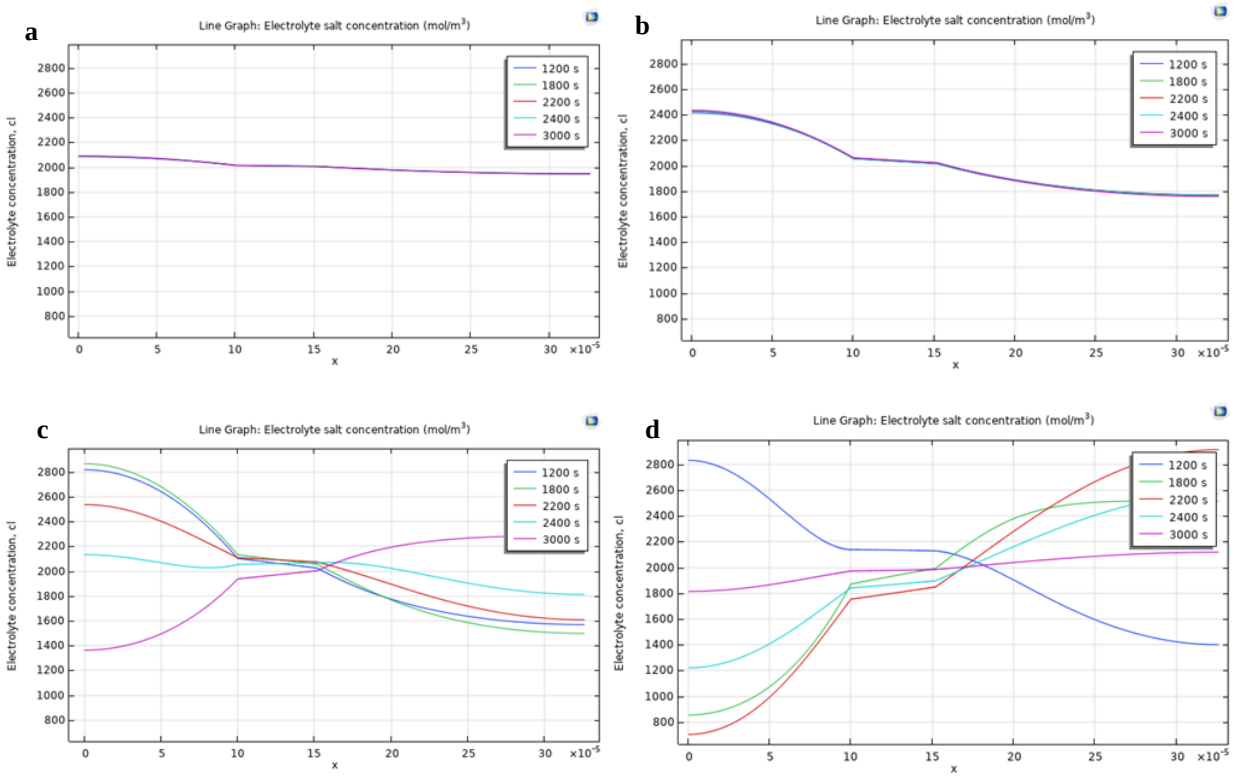

Figure 8. Electrolyte salt concentration for different C-rates: a) 0.1C, b) 0.5C, c) 1C, d) 2C

Table 3. Average electrolyte salt concentration range of battery components for different C-rates

C-Rate	Average Electrolyte Salt Concentration Range of Negative Electrode [0-10]x10^{-5} m	Average Electrolyte Salt Concentration Range of Electrolyte [10-15,2]x10^{-5} m	Average Electrolyte Salt Concentration Range of Positive Electrode [15,2-32,6]x10^{-5} m
0.1	2070 mol/m^3 - 2067 mol/m^3 Difference = 3 mol/m^3	2010 mol/m^3 - 2010 mol/m^3 Difference = 0 mol/m^3	1962 mol/m^3 - 1960 mol/m^3 Difference = 2 mol/m^3
0.5	2340 mol/m^3 - 2330 mol/m^3 Difference = 10 mol/m^3	2040 mol/m^3 - 2035 mol/m^3 Difference = 5 mol/m^3	1820 mol/m^3 – 1810 mol/m^3 Difference = 10 mol/m^3
1	2700 mol/m^3 - 1500 mol/m^3 Difference = 1200 mol/m^3	2080 mol/m^3 - 1970 mol/m^3 Difference = 110 mol/m^3	2250 mol/m^3 - 1600 mol/m^3 Difference = 650 mol/m^3
2	2530 mol/m^3 - 1000 mol/m^3 Difference = 1530 mol/m^3	2130 mol/m^3 - 1800 mol/m^3 Difference = 330 mol/m^3	2650 mol/m^3 - 1650 mol/m^3 Difference = 1000 mol/m^3

Figure 9 reveals that the solid lithium concentration distinction between the surface and center increases with rising C-rate. Generally, the graphs in Figure 9 suggest that the solid lithium concentration of the negative electrode decreases for both the surface and center over time. On the other hand, the solid lithium concentration of the positive electrode increases for both the surface and center over time. Figure 9 and Table 4 clearly show that the difference in average lithium concentration between the center and surface of electrode particles in both electrodes generally increases over time and with rising C-rate.

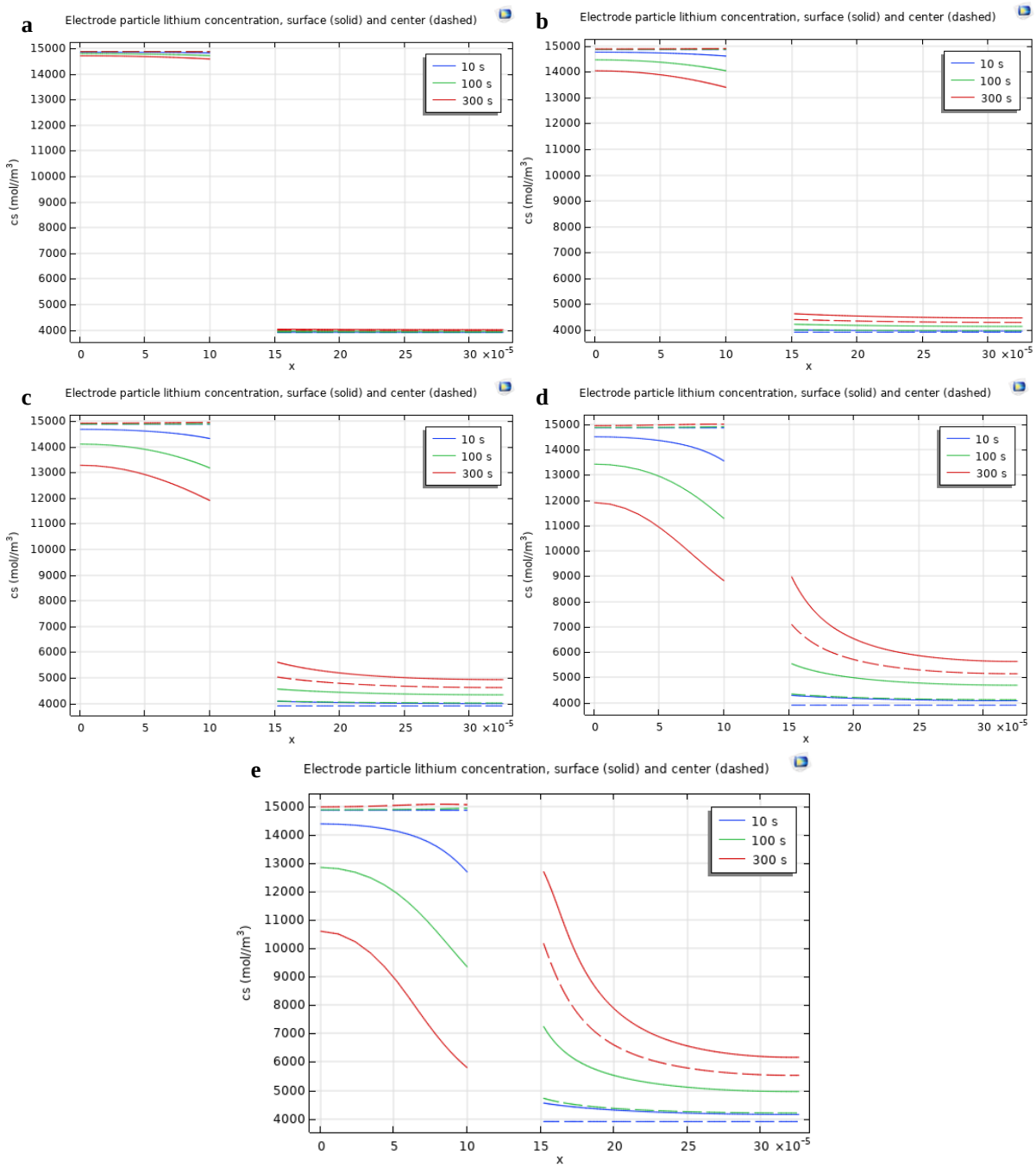

Figure 9. Solid lithium concentration for five different C-rates, a) 0.1C, b) 0.5C, c) 1C, d) 2C, e) 3C

Table 4. Between center and surface, approximate average electrode particle lithium concentration difference of negative and positive electrode for five different C-rates.

C-Rate	Time	Between Center and Surface, Approximate Average Electrode Particle Lithium Concentration Difference of Negative Electrode [0-10]x10^{-5} m	Between Surface and Center Approximate Average Electrode Particle Lithium Concentration Difference of Positive Electrode [15,2-32,6]x10^{-5} m
0.1	10 s.	14870 mol/m^3 - 14840 mol/m^3 Difference = 30 mol/m^3	3910 mol/m^3 - 3900 mol/m^3 Difference = 10 mol/m^3
	100 s.	14870 mol/m^3 - 14775 mol/m^3 Difference = 95 mol/m^3	3950 mol/m^3 - 3910 mol/m^3 Difference = 40 mol/m^3
	300 s.	14870 mol/m^3 - 14680 mol/m^3 Difference = 190 mol/m^3	4020 mol/m^3 - 3980 mol/m^3 Difference = 40 mol/m^3
0.5	10 s.	14870 mol/m^3 - 14740 mol/m^3 Difference = 130 mol/m^3	3950 mol/m^3 - 3900 mol/m^3 Difference = 50 mol/m^3
	100 s.	14870 mol/m^3 - 14380 mol/m^3 Difference = 490 mol/m^3	4150 mol/m^3 - 3950 mol/m^3 Difference = 200 mol/m^3
	300 s.	14900 mol/m^3 - 13900 mol/m^3 Difference = 1000 mol/m^3	4500 mol/m^3 - 4300 mol/m^3 Difference = 200 mol/m^3
1	10 s.	14870 mol/m^3 - 14600 mol/m^3 Difference = 270 mol/m^3	4000 mol/m^3 - 3900 mol/m^3 Difference = 10 mol/m^3
	100 s.	14880 mol/m^3 - 13900 mol/m^3 Difference = 980 mol/m^3	4365 mol/m^3 - 4030 mol/m^3 Difference = 335 mol/m^3
	300 s.	14920 mol/m^3 - 12900 mol/m^3 Difference = 2020 mol/m^3	5000 mol/m^3 - 4670 mol/m^3 Difference = 330 mol/m^3
2	10 s.	14870 mol/m^3 - 14370 mol/m^3 Difference = 500 mol/m^3	4105 mol/m^3 - 3900 mol/m^3 Difference = 205 mol/m^3
	100 s.	14890 mol/m^3 - 12950 mol/m^3 Difference = 1940 mol/m^3	4778 mol/m^3 - 4150 mol/m^3 Difference = 628 mol/m^3
	300 s.	14980 mol/m^3 - 10930 mol/m^3 Difference = 4050 mol/m^3	5860 mol/m^3 - 5300 mol/m^3 Difference = 560 mol/m^3
3	10 s.	14870 mol/m^3 - 14155 mol/m^3 Difference = 715 mol/m^3	4200 mol/m^3 - 3900 mol/m^3 Difference = 300 mol/m^3
	100 s.	14897 mol/m^3 – 12016 mol/m^3 Difference = 2881 mol/m^3	5110 mol/m^3 - 4250 mol/m^3 Difference = 860 mol/m^3
	300 s.	15040 mol/m^3 - 8967 mol/m^3 Difference = 6073 mol/m^3	6560 mol/m^3 - 5790 mol/m^3 Difference = 770 mol/m^3

Figure 10 shows the discharge curve comparisons for the five different C-rates (0.1C, 0.5C, 1C, 2C, and 3C). According to Ohm's law, voltage and current exhibit a direct relationship. Hence, when the circuit demands a higher current, the battery will release more voltage [15].

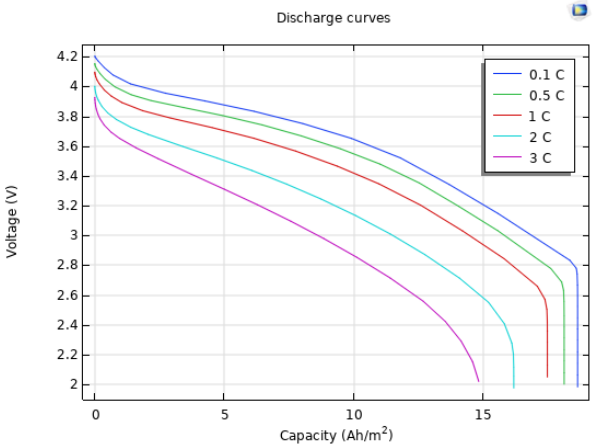

Figure 10. Discharge curve comparison for five different C-rates

4. Conclusions

Understanding the relationship between functional aspects and design choices plays a critical role in the development of battery technology. In the foreseeable future, the modelling of energy storage devices and systems will remain a highly relevant topic, and Li-ion batteries are projected to remain a relevant chemistry due to the high energy and power density with respect to other battery types. In this study, a 1D isothermal lithium-ion battery is investigated under different C-rates using the COMSOL Multiphysics software battery and design module. This research presented that when the C-rates increase, over time the electrolyte and electrode voltage range, electrolyte salt concentration differences of battery components, and differences of surface and center electrode particle lithium concentrations rise.

Acknowledgments

Elif Kaya acknowledges the financial support provided by the Republic of Türkiye Ministry of National Education for her PhD at the University of Modena and Reggio Emilia. Luca Reina acknowledges the financial support provided by European Union, NextGenerationEU and by CNH Industrial for PhD Scholarship funding (CUP: E93C23001710008, DOT1317193 - INGEGNERIA MECCANICA E DEL VEICOLO), and the technical support by R&D CFD S.R.L. Alessandro d'Adamo acknowledges the financial support provided by European Union, NextGenerationEU - National Sustainable Mobility Center - MOST, CN00000023, Italian Ministry of University and Research, Spoke 12 (CUP: E93C22001070001).

5. References

[1] Kaya, A. F., Acir, A., & Kaya, E. (2023). Numerical investigation of wind-lens combinations for improving aerodynamic performance of an elliptical-bladed Savonius wind turbine. *Journal of the Brazilian Society of Mechanical Sciences and Engineering*, *45*(6), 309.

[2] https://www.slideserve.com/adrina/bataryalar

[3] Silberberg, M. (2014). *Chemistry: The molecular nature of matter and change*. McGraw-Hill Higher Education.

[4] Li, A., Yuen, A. C. Y., Wang, W., De Cachinho Cordeiro, I. M., Wang, C., Chen, T. B. Y., ... & Yeoh, G. H. (2021). A review on lithium-ion battery separators towards enhanced safety performances and modelling approaches. *Molecules*, *26*(2), 478.

[5] https://evreporter.com/understanding-memory-effect-in-lithium-ion-batteries/

[6] Leißing, M., Horsthemke, F., Wiemers-Meyer, S., Winter, M., Niehoff, P., & Nowak, S. (2021). The Impact of the C-Rate on Gassing During Formation of NMC622 II Graphite Lithium-Ion Battery Cells. *Batteries & Supercaps*, *4*(8), 1344-1350.

[7] Snyder, C. (2016). *The effects of charge/discharge rate on capacity fade of lithium ion batteries*. Rensselaer Polytechnic Institute.

[8] Somerville, L., Bareño, J., Trask, S., Jennings, P., McGordon, A., Lyness, C., & Bloom, I. (2016). The effect of charging rate on the graphite electrode of commercial lithium-ion cells: A post-mortem study. *Journal of Power Sources*, *335*, 189-196.

[9] Wang, J., Liu, P., Hicks-Garner, J., Sherman, E., Soukiazian, S., Verbrugge, M., ... & Finamore, P. (2011). Cycle-life model for graphite-LiFePO4 cells. *Journal of power sources*, *196*(8), 3942-3948.

[10] Tran, T. D., Feikert, J. H., Pekala, R. W., & Kinoshita, K. (1996). Rate effect on lithium-ion graphite electrode performance. *Journal of applied electrochemistry*, *26*, 1161-1167.

[11] Li, J., Wang, D., & Pecht, M. (2019). An electrochemical model for high C-rate conditions in lithium-ion batteries. *Journal of Power Sources*, *436*, 226885.

[12] Zheng, H., Li, J., Song, X., Liu, G., & Battaglia, V. S. (2012). A comprehensive understanding of electrode thickness effects on the electrochemical performances of Li-ion battery cathodes. *Electrochimica Acta*, *71*, 258-265.

[13] 1D Isothermal Lithium Ion Battery. COMSOL Inc. www.comsol.com. Web https://www.comsol.com/model/1d-isothermal-lithium-ion-battery-686

[14] Lu, J. (2013). *Development of fast one-dimensional model for prediction of coupled electrochemical-thermal behavior of Lithium-ion batteries* (Doctoral dissertation, The Ohio State University).

[15] Huber, I. S. (2017). Using COMSOL to Model a 1-D Lithium-Ion Battery.

[16] Linden, D. (1995). Handbook of batteries. In *Fuel and energy abstracts* (Vol. 4, No. 36, p. 265).

[17] Doyle, M., Newman, J., Gozdz, A. S., Schmutz, C. N., & Tarascon, J. M. (1996). Comparison of modeling predictions with experimental data from plastic lithium ion cells. *Journal of the Electrochemical Society*, *143*(6), 1890.